Electronic Supplementary Material (ESI) for Journal of Materials Chemistry C
This journal is © The Royal Society of Chemistry 2013

Multifunctional Micro- and Nanosized Metal-Organic Frameworks Assembled from Bisphosphonates and Lanthanides

Sérgio M. F. Vilela,[1] Duarte Ananias,[1,2] José A. Fernandes,[1] Patrícia Silva,[1] Ana C. Gomes,[1] Nuno J. O. Silva,[2] Marcelo O. Rodrigues,[1,3] João P. C. Tomé,[4] Anabela A. Valente,[1] Paulo Ribeiro-Claro,[1] Luís D. Carlos,[2] João Rocha,[1] and Filipe A. Almeida Paz[1,]*

A contribution from

[1] Department of Chemistry, CICECO, University of Aveiro, 3810-193 Aveiro, Portugal
[2] Department of Physics, CICECO, University of Aveiro, 3810-193 Aveiro, Portugal
[3] LIMA-Laboratório de Inorgânica e Materiais, University of Brasilia (IQ-UnB), Campus Universitário Darcy Ribeiro, CEP 70904970, P.O. Box 4478, Brasilia-DF, Brazil
[4] Department of Chemistry, QOPNA, University of Aveiro, 3810-193 Aveiro, Portugal

Electronic Supporting Information

To whom correspondence should be addressed:

Dr. Filipe A. Almeida Paz
Department of Chemistry, CICECO
University of Aveiro
3810-193 Aveiro
Portugal

E-mail: filipe.paz@ua.pt
FAX: +351 234 370084
Telephone: +351 234 370200 (Extension 23553)

Contents

1 – Synthesis and Structural Characterization

1.1 – [Ln(Hpmd)(H_2O)] Coordination Polymers

2 – Vibrational Spectroscopy

2.1 – Experimental Data

2.2 – Theoretical Data

1 – Synthesis and Structural Characterization

1.1 – [Ln(Hpmd)(H_2O)] Coordination Polymers

1.1.1 – [Gd(Hpmd)(H_2O)] – Rietveld Refinement

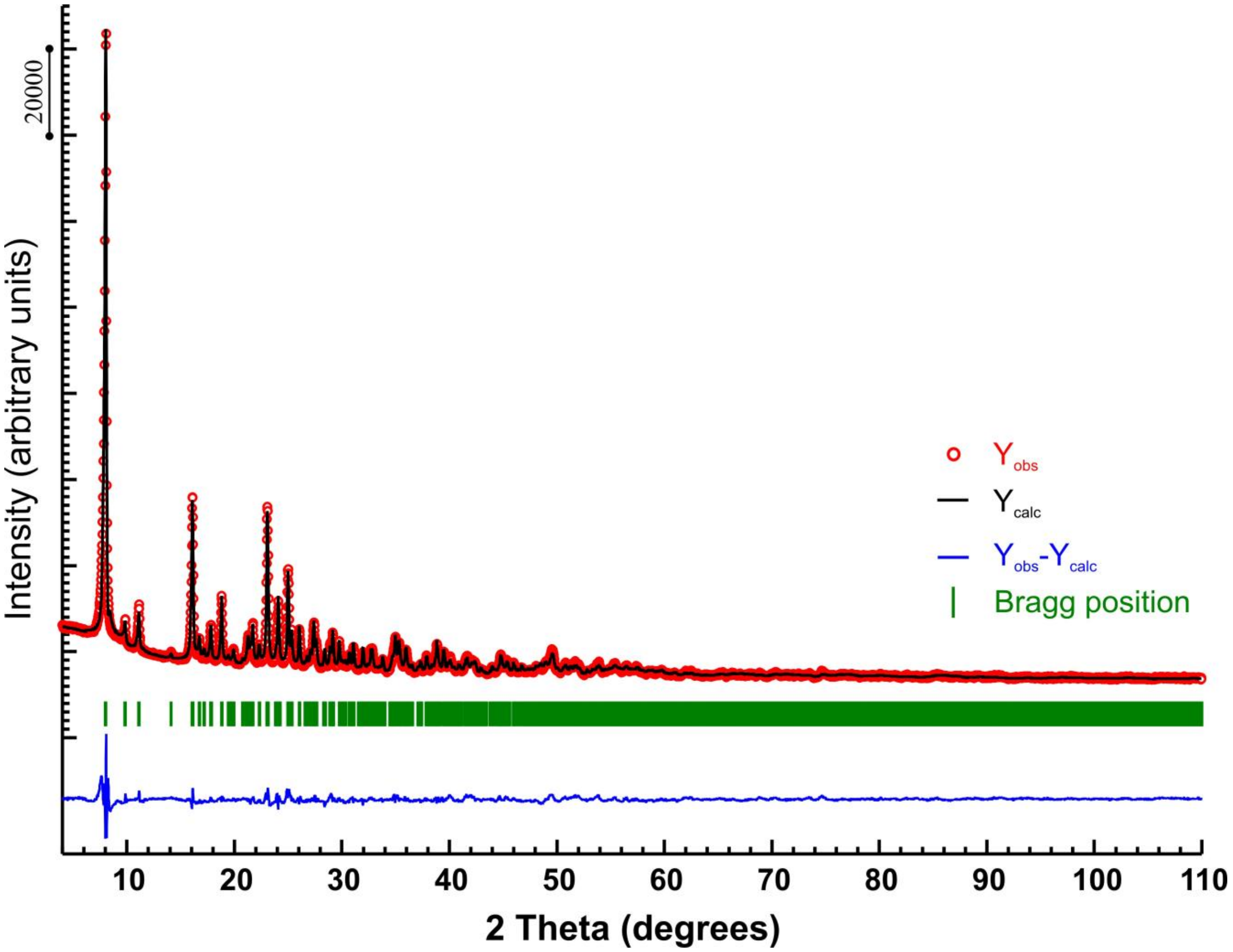

Figure S1 - Final Rietveld plot (laboratory powder X-ray diffraction data) of [Gd(Hpmd)(H_2O)] (**2**). Observed data points are indicated as red circles, the best-fit profile (upper trace) and the difference pattern (lower trace) are drawn as solid black and blue lines, respectively. Green vertical bars indicate the angular positions of the allowed Bragg reflections. Refinement details are given in Table 1 (in the main paper).

1.1.2 – [Tb(Hpmd)(H_2O)] – Rietveld Refinement

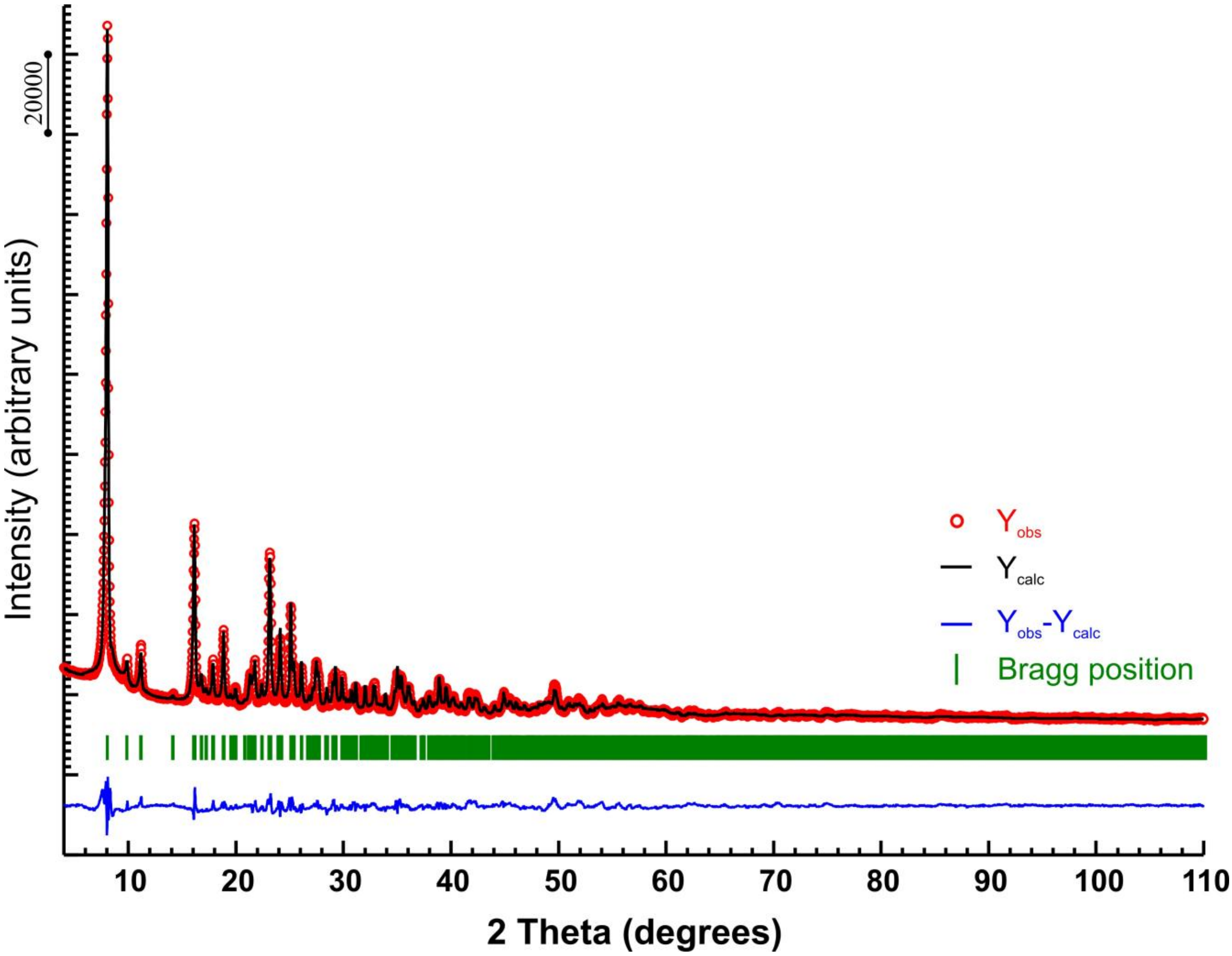

Figure S2 - Final Rietveld plot (laboratory powder X-ray diffraction data) of [Tb(Hpmd)(H_2O)] (**3**). Observed data points are indicated as red circles, the best-fit profile (upper trace) and the difference pattern (lower trace) are drawn as solid black and blue lines, respectively. Green vertical bars indicate the angular positions of the allowed Bragg reflections. Refinement details are given in Table 1 (in the main paper).

1.1.3 – SEM of [Eu(Hpmd)(H_2O)] prepared under microwave irradiation

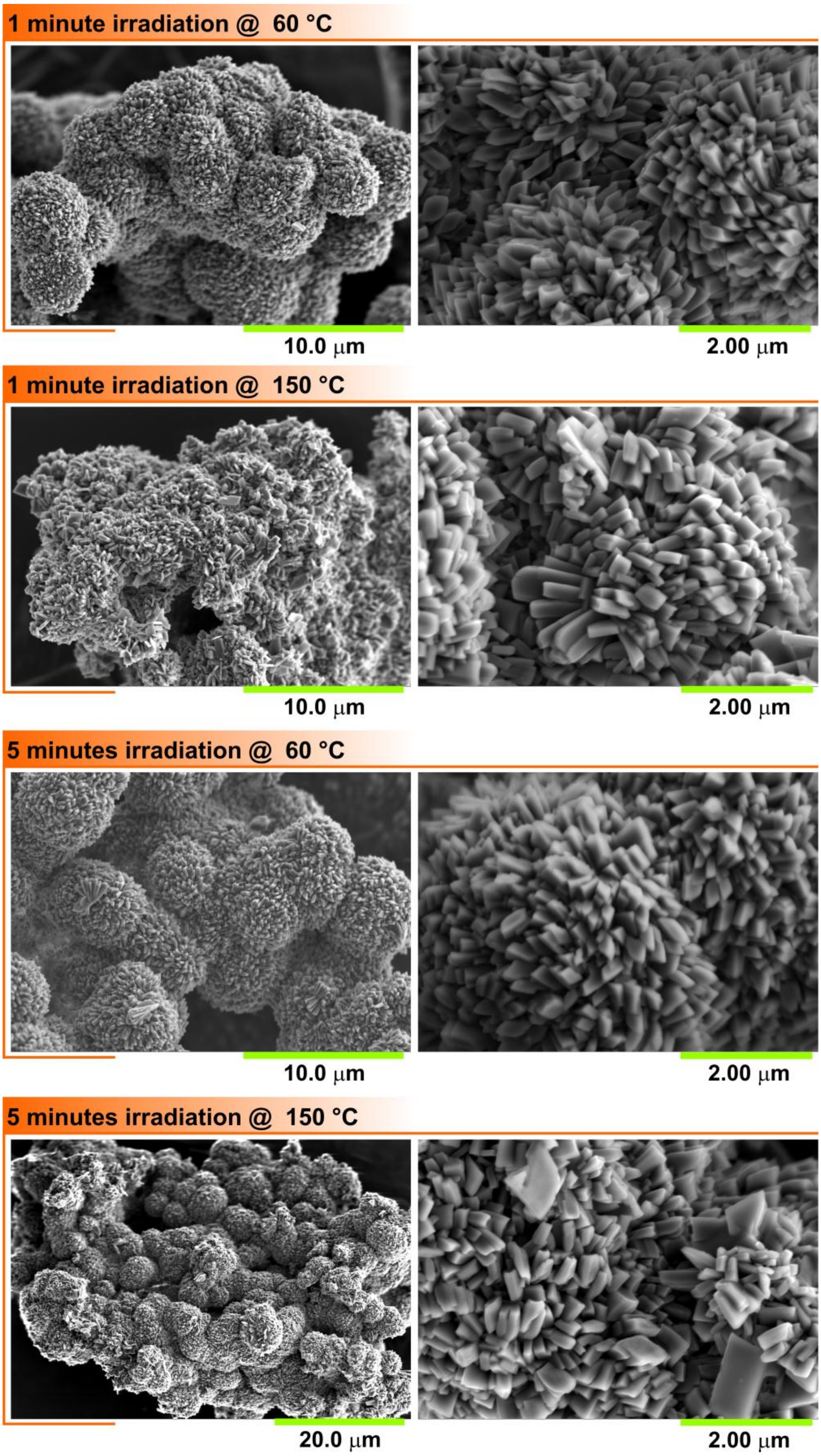

Figure S3 - SEM images of material [Eu(Hpmd)(H_2O)] (**1**) prepared using microwave heating (power 50 W).

1.1.4 – Ultrasound-Assisted Synthesis: Isolated Nanoparticles

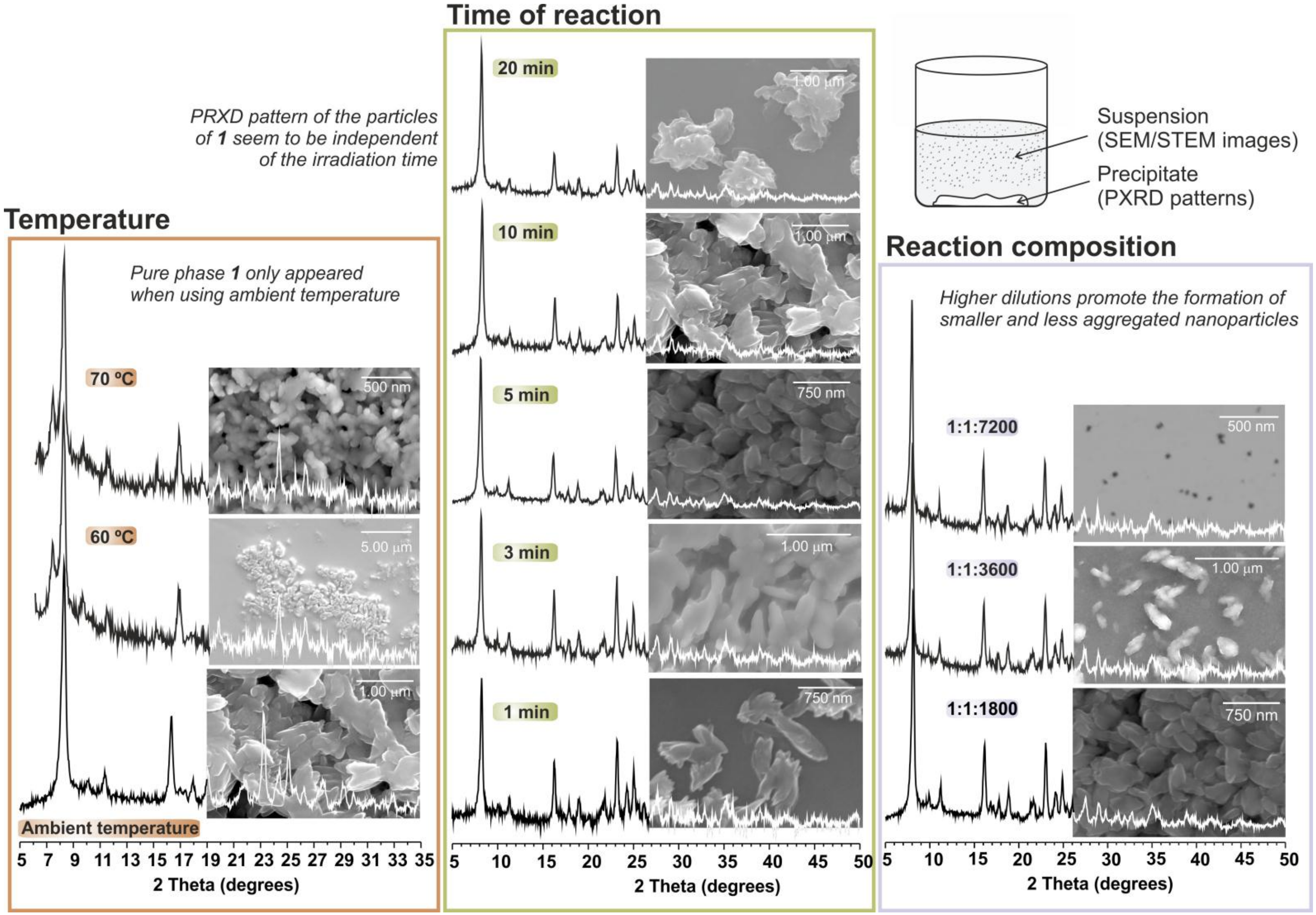

Figure S4 - Optimization of the ultrasound-assisted synthesis of compound [Eu(Hpmd)(H_2O)] (**1**) so to prepare isolated nanoparticles.

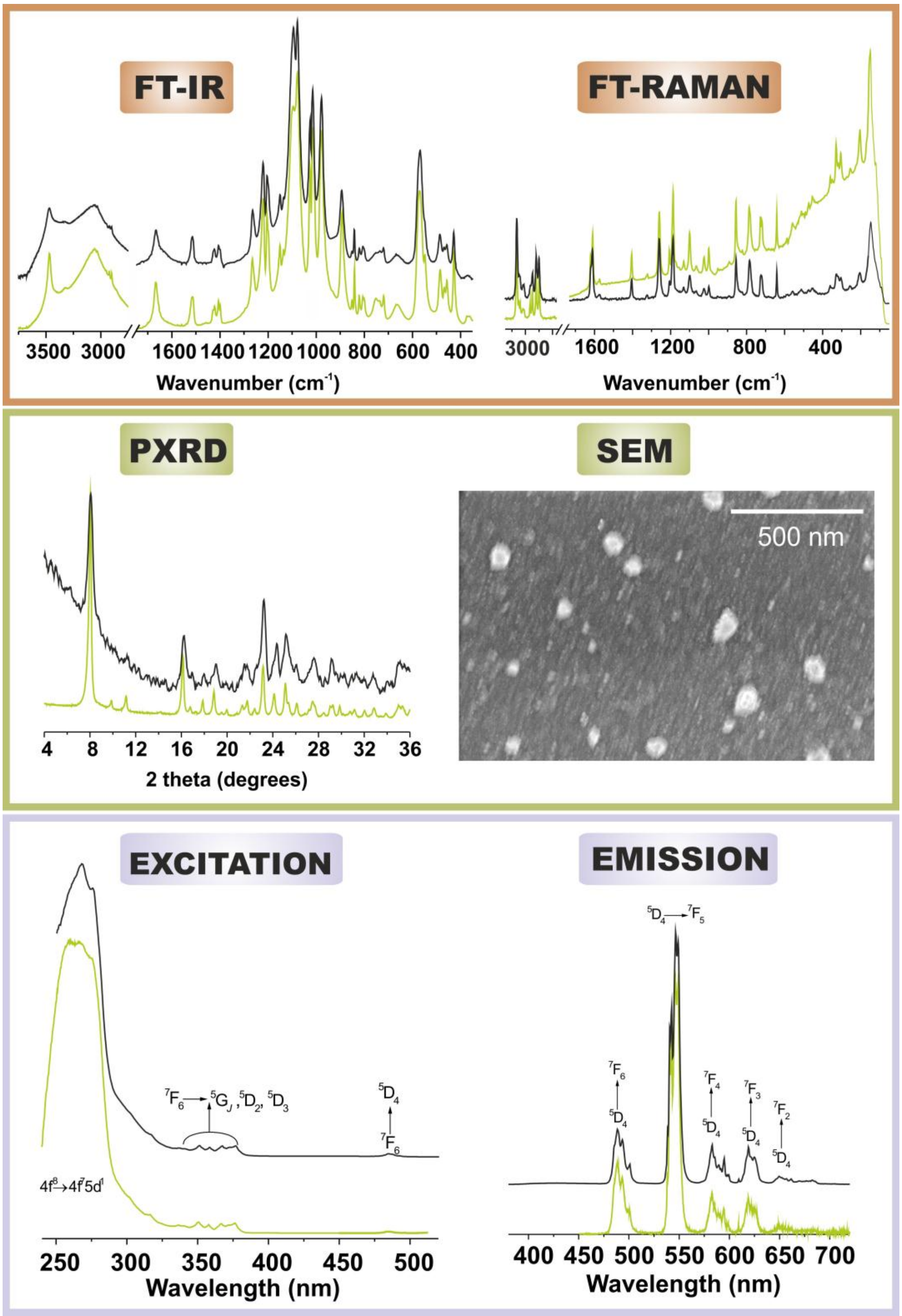

Figure S5 - Structural data for [Eu(Hpmd)(H_2O)] (**1**): nano-sized crystals obtained using ultrasonic irradiation (black line) and the microcrystalline bulk material (green line).

1.1.5 – Thermogravimetry

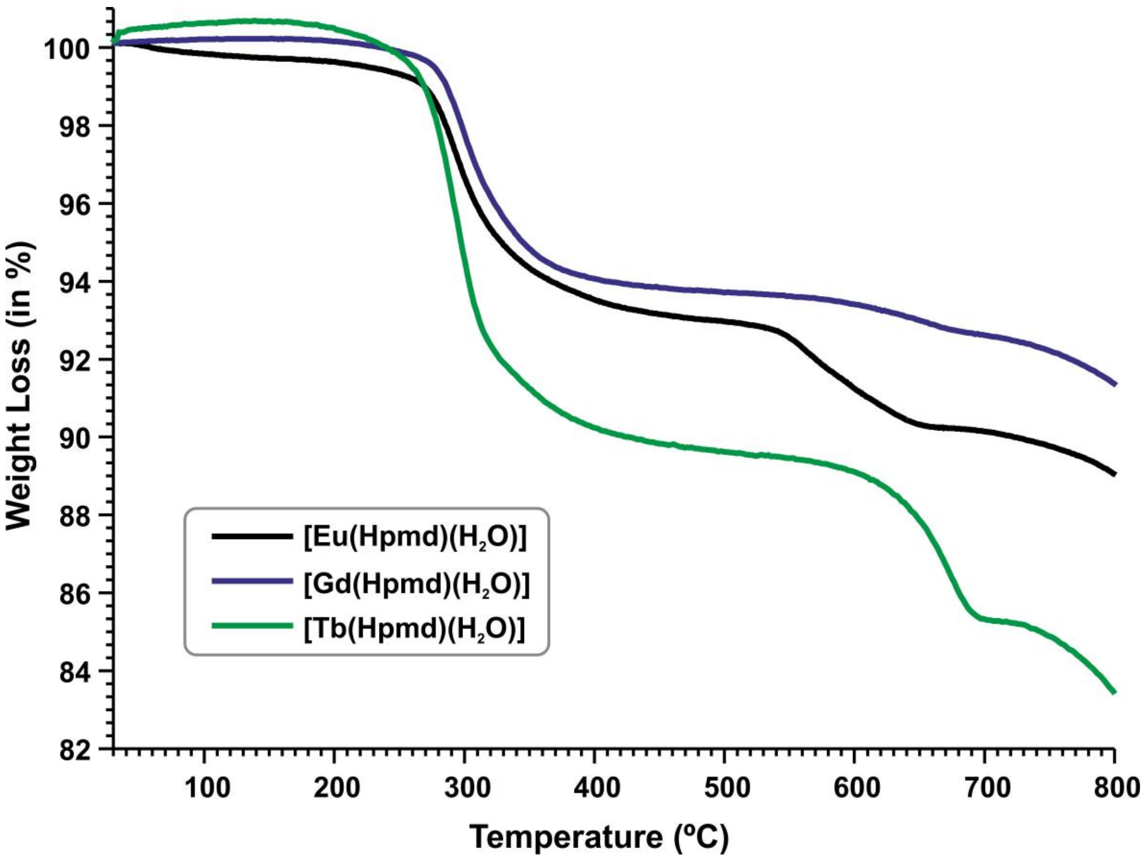

Figure S6 - Thermograms of [LnHpmd)(H_2O)] materials between ambient temperature and 800 ºC.

2 – Vibrational Spectroscopy

2.1 – Experimental Data

2.1.1 – FT-IR

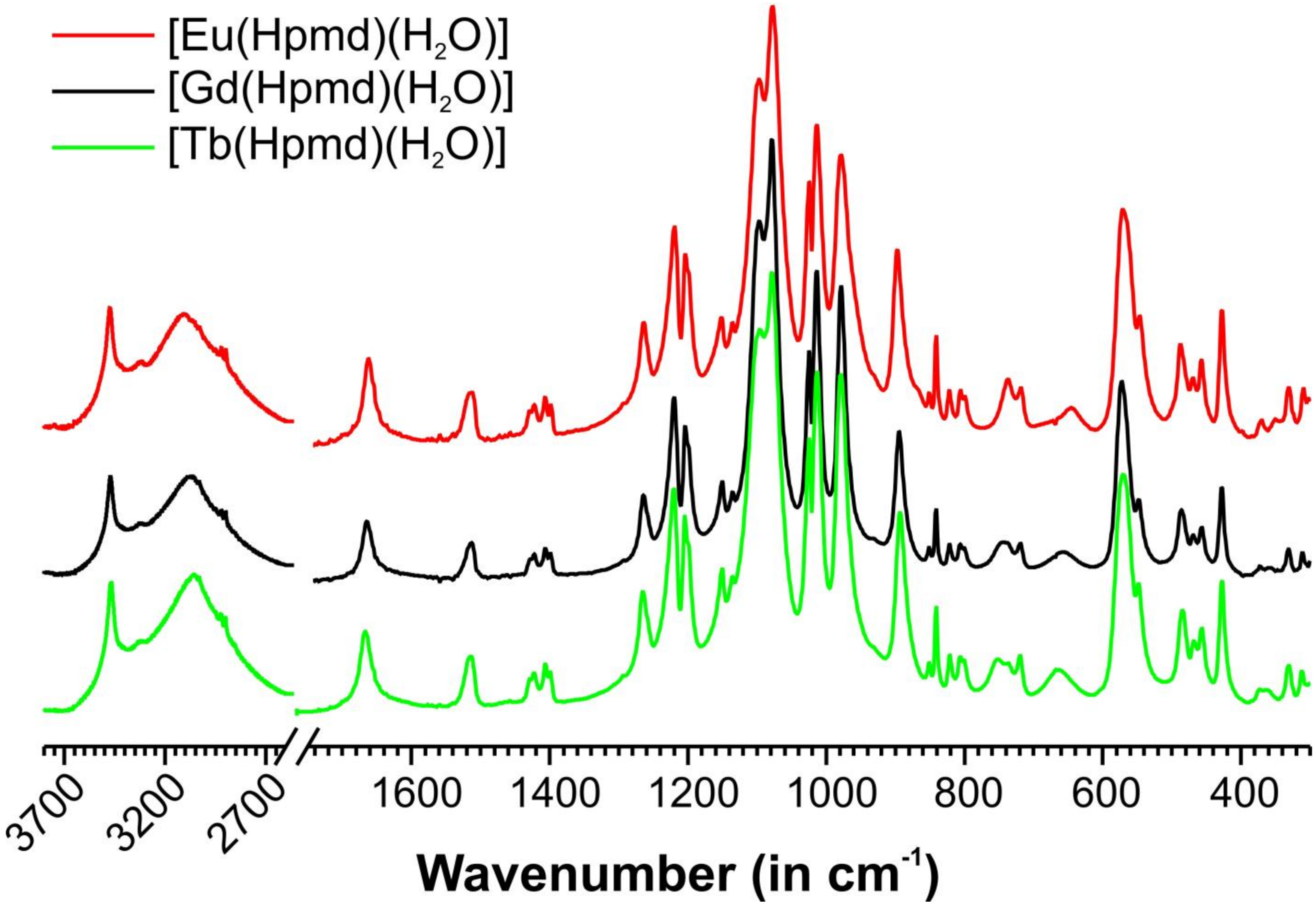

Figure S7 - FT-IR spectra (in absorbance, arbitrary units) of [LnHpmd)(H_2O)] materials collected from KBr pellets.

2.1.2 – FT-Raman

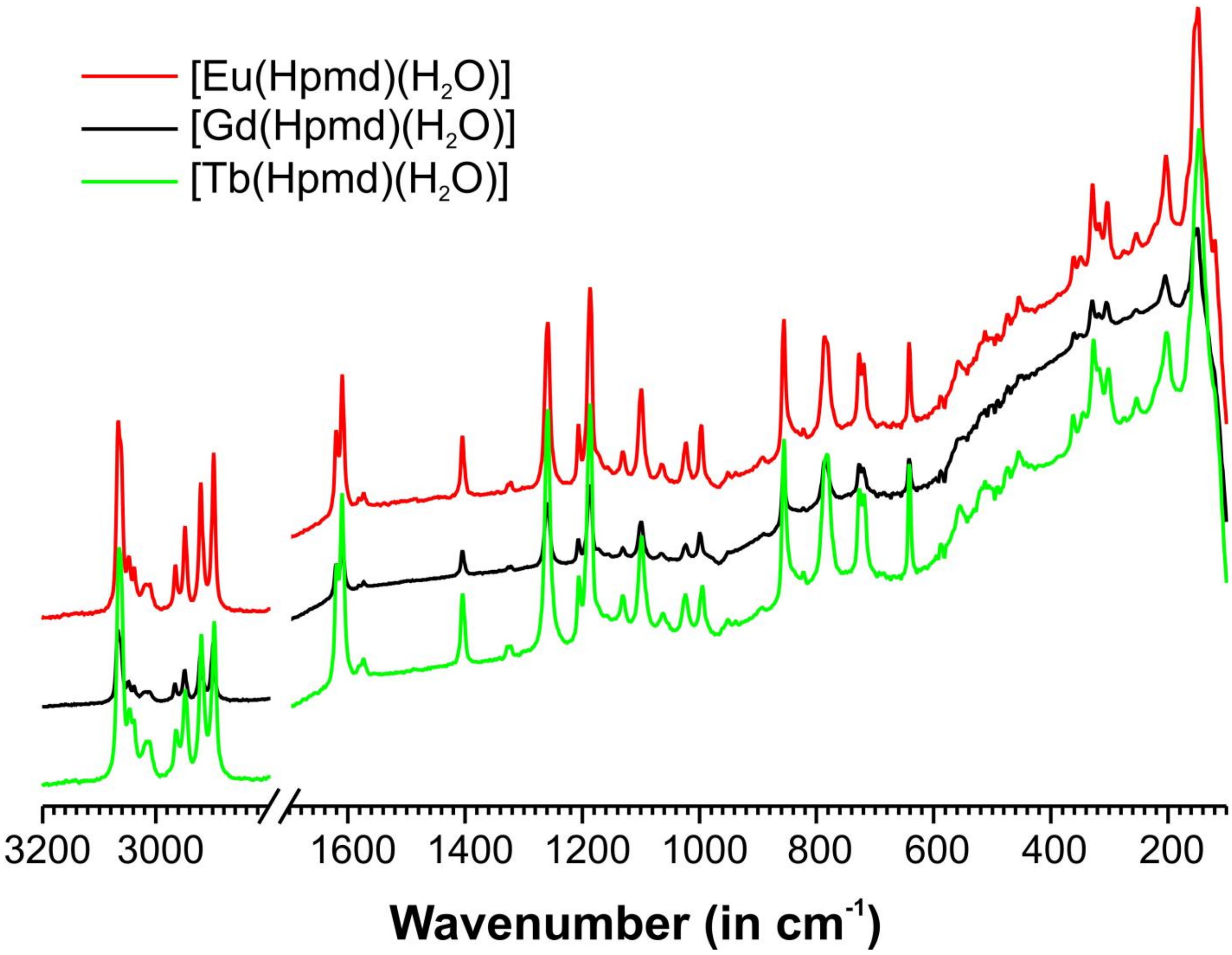

Figure S8 - FT-Raman spectra (in absorbance, arbitrary units) of [LnHpmd)(H_2O)] materials. The spectra have a large fluorescence band below 2500 cm^{-1}.

2.2 – Theoretical Data

2.2.1 – Optimization boxes

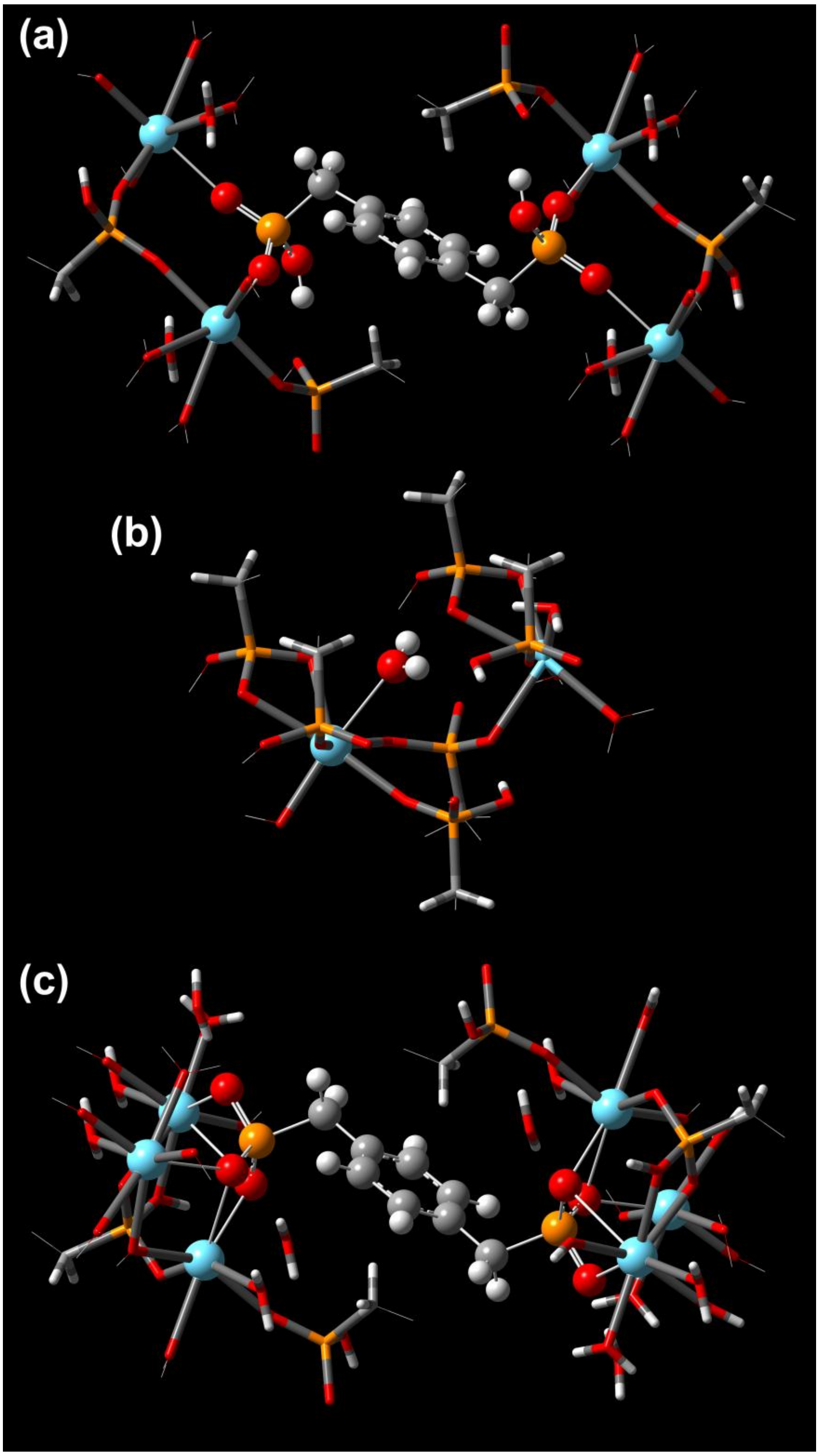

Figure S9 - Model geometries for the **(a)** hydrogenophosphonate, **(b)** coordinated water and **(c)** phosphonate moieties and their neighbourhoods. The first layer is represented in "ball and stick" mode and depicts the optimized portion for which the vibrations were determined. The second layer is depicted in "tube" mode and corresponds to the fixed crystallographic atom positions. The third layer is shown in "wireframe" mode and corresponds to included hydrogen atoms which are needed for fulfill the connectivity of the terminal atoms of the second layer.

2.2.2 – FT-IR tabulated data: comparison between experimental and theoretical

Table S1. Comparison between the experimental and theoretical FT-IR bands for compound **3**.

Experimental[a]	*Calculated*	*Fragment*[b]	*Assignments*
363; 372	367	P	$\tau(PO_3) + \rho(CH_2)$
428*m*	410	H	$\tau(PO_3) + \rho(CH_2)$
	433	H	$\tau(PO_3) + \rho(CH_2)$
457	468	P	$\delta(PO_3) + \gamma(Ph)$
469	478	H	$\delta(PO_3) + \gamma(Ph)$
488	494	P	$\delta(PO_3) + \gamma(Ph)$
	495	W	$\omega(H_2O)$
548	531	P	$\delta(PO_3) + \gamma(Ph)$
572*m*	573	P	$\delta(PO_3) + \gamma(Ph)$
663	648	W	$\tau(H_2O)$
737[c]	707	H	$\gamma(POH)$
718	723	P	$\gamma(CH)$
752	746	H	$\gamma(CH)$
799; 806 822; 840	806	H	$\delta(Ph)$
	839	P	$\rho(CH_2)$
	845	H	$\rho(CH_2)$
866	881	H	$\rho(CH_2) + \gamma(CH)$
897*m*	912	H	$\rho(CH_2) + \gamma(CH)$
979*s*	959	P	$\nu(PO_3) + \nu(PC)$
1014*s*; 1025*m*	992	P	$\nu(PO_3) + \omega(CH_2)$
1078*vs*	1075	P	$\nu(PO_3) + \rho(CH_2)$
1097*s*	1075	H	$\nu(PO_3) + \tau(CH_2)$
1136	1116	H	$\tau(CH_2)$
1152	1146	H	$\delta(POH)$
1219*m*[c]	1215	H	$\delta(POH) + \omega(CH_2)$
1203*m*	1247	H	$\delta(CH) + \omega(CH_2)$
1264	1289	H	$\delta(CH) + \omega(CH_2)$
1398	1462	H	$\delta(CH) + \tau(CH_2)$
1407	1464	P	$\delta(CH_2) + \nu(Ph)$
1422	1487	P	$\delta(CH_2) + \nu(Ph)$
1429	1492	H	$\delta(CH_2)$
1513	1560	H	$\nu(Ph)$
1516	1564	P	$\nu(Ph)$
1667	1605	W	$\delta(H_2O)$
2900	3044	P	$\nu(CH_2)$
2922	3066	H	$\nu(CH_2)$
3054*b*	3438	H	$\nu(POH)$
3468*m*	3606; 3791	W	$\nu(H_2O)$

[a] Peaks are weak unless they are assigned as *s* – strong, *b* - broad or *m* - medium.

[b] P and H correspond to the phosphonate and hydrogenophosphonate ligands, respectively; W corresponds to the coordinated water.

[c] Assignments based on calculated vibrational modes and comparison between deuterated and non-deuterated samples.

2.2.3 – FT-Raman tabulated data: comparison between experimental and theoretical

Table S2. Comparison between the experimental and theoretical FT-Raman bands for compound **3**.

Experimental [a]	*Calculated*	*Fragment* [b]	*Assignments*
318	321	P	γ(Ph) + ρ(PO_3)
329*m*	326	H	γ(Ph) + ρ(PO_3)
351	343	P	ρ(PO_3) + ρ(CH_2)
360	378	P	ρ(CH_2) + δ(Ph)
642*m*	658	H and P	δ(Ph)
711	713	H	γ(POH) + γ(Ph)
720*m*	733	P	γ(Ph)
727*m*	745	H	γ(POH) + γ(Ph)
786*m*	783	P	γ(Ph) + ν(PO_3)
	789	H	γ(POH) + γ(Ph)
857*s*	873	P	δ(Ph)
	860	H	δ(Ph)
999	964	P	ν(PO_3)
1024	991	P	ν(PO_3) + γ(CH)
1065	1075	P	ν(PO_3)
1100*m*	1079	H	τ(CH_2)
1131	1141 and 1153	H	τ(CH_2) + δ(POH)
1186*s*	1213	H	ω(CH_2) + δ(POH)
1207	1237 and 1241	H	δ(CH_2)
1260*s*	1317	P	ω(CH_2) + ν(Ph)
	1286	H	ω(CH_2) + ν(Ph)
1405*m*	1481	P	δ(CH_2)
	1491	H	δ(CH_2)
1572	1605	W	δ(H_2O)
1581	1638	P	ν(Ph)
	1631	H	ν(Ph)
1610*s*	1677	H	ν(Ph)
1620	1686	P	ν(Ph)
2998*m*	3043	P	ν_s(CH_2)
2921*m*	3066	H	ν_s(CH_2)
2949	3114	P	ν_a(CH_2)
2960	3127	H	ν_a(CH_2)
3039	3189	P	ν(CH)
3048	3192	H	ν(CH)
3066*s*	3218	H and P	ν(CH)

[a] Peaks are weak unless they are assigned as *s* - strong or *m* - medium.

[b] P and H correspond to the phosphonate and hydrogenophosphonate ligands, respectively; W corresponds to the coordinated water. The 375-630 cm^{-1} range was affected by noise related to the fluorescence band.

3 – Magnetism

This section contains all the equations used in the description of the magnetic properties of [Eu(Hpmd)(H_2O)] (**1**) and [Gd(Hpmd)(H_2O)] (**2**).

For Equations S1 to S3 please refer to a general text book on magnetism and molecular magnetism.[1]

Equation S1 (Brillouin law):

$$M = Ng\mu_B S B_S(x)$$

with

$$B_S(x) = \frac{1}{S}\left[(S+\tfrac{1}{2})\operatorname{cotgh}(S+\tfrac{1}{2})x - \tfrac{1}{2}\operatorname{cotgh}\tfrac{1}{2}x\right]$$
$$x = Ng\mu_B / kT$$

where g is the Landé factor (equal to 2 in the case of Gd^{3+}), μ_B is the Bohr magneton and k is the Boltzman constant. N is the density of magnetic ions, whose units depend on the units of M, being equal to **1** in the case of data presented in Figure 8a (in the main paper).

Equation S2 (Curie-Weiss law with a constant term):

$$\chi = \frac{Ng^2\mu_B^2}{3k(T-\theta)} S(S+1) + \chi_0$$

Equation S3 (Van Vleck formula applied to Eu^{3+}):

$$\chi = \frac{N\mu_B^2}{3kTx}[24 + (27x/2 - 3/2)\exp(-x) + (135x/2 - 5/2)\exp(-3x)$$
$$+ (189x - 7/2)\exp(-6x) + (405x - 9/2)\exp(-10x) + (1485x/2 - 11/2)\exp(-15x)$$
$$+ (2457x/2 - 13/2)\exp(-21x)]/[1 + 3\exp(-x) + 5\exp(-3x) + 7\exp(-6x) + 9\exp(-10x)$$
$$+ 11\exp(-15x) + 13\exp(-21x)]$$

with

$$x = \lambda / kT$$

4 – Photoluminescence

Based on the emission spectra, $^5D_0$ lifetimes and empirical radiative and non-radiative transition rates, the $^5D_0$ quantum efficiency, q[2] has been determined for compounds **1** and **1_D**. The number of coordinated water molecules was also evaluated. Assuming that only non-radiative and radiative processes are involved in the depopulation of the $^5D_0$ state, q is given by:

$$q = \frac{k_r}{k_r + k_{nr}} \quad \text{(Equation S4)}$$

where k_r and k_{nr} are the radiative and non-radiative transition probabilities, respectively, and $k_{exp}=\tau_{exp}^{-1}$ $(k_r + k_{nr})$ is the experimental transition probability. The emission intensity, I, taken as the integrated intensity S of the emission lines for the $^5D_0 \rightarrow {}^7F_{0-6}$ transitions, is given by:

$$I_{i \rightarrow j} = \hbar w_{i \rightarrow j} A_{i \rightarrow j} N_i \equiv S_{i \rightarrow j} \quad \text{(Equation S5)}$$

where i and j represent the initial ($^5D_0$) and final ($^7F_{0-6}$) levels, respectively, $\hbar w_{i \rightarrow j}$ is the transition energy, $A_{i \rightarrow j}$ the Einstein coefficient of spontaneous emission and N_i the population of the $^5D_0$ emitting level. [2] Because the $^5D_0 \rightarrow {}^7F_{5,6}$ transitions are not observed experimentally, their influence on the depopulation of the $^5D_0$ excited state may be neglected and, thus, the radiative contribution is estimated based only on the relative intensities of the $^5D_0 \rightarrow {}^7F_{0-4}$ transitions. The emission integrated intensity, S, of the $^5D_0 \rightarrow {}^7F_{0-4}$ transitions has been measured for compounds **1** and **2** at 298 K.

Because the $^5D_0 \rightarrow {}^7F_1$ transition does not depend on the local ligand field seen by the Eu^{3+} ions (due to its dipolar magnetic nature) it may be used as a reference for the whole spectrum, *in vacuo* $A(^5D_0 \rightarrow {}^7F_1)=14.65\ s^{-1}$,[3] and k_r is given by:

$$k_r = A_{0 \rightarrow 1} \frac{\hbar\omega_{0 \rightarrow 1}}{S_{0 \rightarrow 1}} \sum_{J=0}^{4} \frac{S_{0-J}}{\hbar\omega_{0-J}} \quad \text{(Equation S6)}$$

where A_{0-1} is the Einstein coefficient of spontaneous emission between the $^5D_0$ and the $^7F_1$ levels. An average index of refraction of 1.5 was considered for both samples, leading to $A(^5D_0 \rightarrow {}^7F_1) \approx 50\ s^{-1}$.[4]

The number of water molecules (n_w) coordinated to Eu^{3+} may be determined using the empirical formula of Horrocks and Sudnick (intrinsic error of ±0.5) using the ambient temperature lifetimes:[5]

$$n_w = A \bullet \left(\frac{1}{\tau_{H_2O} - 1} - \frac{1}{\tau_{D_2O} - w} \right) \quad \text{(Equation S7)}$$

where A = 1.11 and W = 0.33 for Eu^{3+}.

5 – References

1. (a) O. Kahn, *Molecular Magnetism*, *Chapter 1*, Wiley-VCH, 1993; (b) O. Kahn, *Molecular Magnetism*, *Chapter 2*, Wiley-VCH, 1993.
2. (a) L. D. Carlos, Y. Messaddeq, H. F. Brito, R. A. S. Ferreira, V. D. Bermudez and S. J. L. Ribeiro, *Adv. Mater. (Weinheim, Ger.)*, 2000, **12**, 594-598; (b) O. L. Malta, H. F. Brito, J. F. S. Menezes, F. R. G. E. Silva, S. Alves, F. S. Farias and A. V. M. deAndrade, *J. Lumin.*, 1997, **75**, 255-268; (c) O. L. Malta, M. A. C. dos Santos, L. C. Thompson and N. K. Ito, *J. Lumin.*, 1996, **69**, 77-84.
3. M. H. V. Werts, R. T. F. Jukes and J. W. Verhoeven, *Phys. Chem. Chem. Phys.*, 2002, **4**, 1542-1548.
4. M. F. Hazenkamp and G. Blasse, *Chem. Mater.*, 1990, **2**, 105-110.
5. R. M. Supkowski and W. D. Horrocks, *Inorg. Chim. Acta*, 2002, **340**, 44-48.